Journal of Alloys and Compounds 509 (2011) 4167–4170

Contents lists available at ScienceDirect

Journal of Alloys and Compounds

journal homepage: www.elsevier.com/locate/jallcom

Influence of Li and Nb ratios on the defect structure and exposure energy in $LiNbO_3$:Fe:Mn:Zr crystals

Chao Xu[a], Chunhui Yang[a,*], Li Dai[b], Liang Sun[a], Yuheng Xu[a], Liangcai Cao[c]

[a] School of Chemical Engineering and Technology, Harbin Institute of Technology, Harbin 150001, PR China
[b] Applied Science College, Harbin University of Science and Technology, Harbin 150080, PR China
[c] State Key Laboratory of Precision Measurement Technology and Instruments, Tsinghua University, Beijing 100084, PR China

ARTICLE INFO

Article history:
Received 19 November 2010
Received in revised form 4 January 2011
Accepted 7 January 2011
Available online 12 January 2011

Keywords:
$LiNbO_3$:Mn:Fe:Zr crystal
Li/Nb ratio
Light-induced scattering
Distribution coefficient

ABSTRACT

A series of $LiNbO_3$:Fe:Mn:Zr crystals with different ratios of Li/Nb in the melt (0.94,1.05,1.20 and 1.38, respectively) were grown by the conventional Czochralski technique. The ultraviolet–visible spectra were measured in order to analyze the defect structure of the crystals. The measurement of the Zr concentrations and Li/Nb ratios in the crystals was carried out with an inductively coupled plasma atomic emission spectrometer. The light-induced scattering was investigated as a function of exposure energy. The results showed that the ability to resist the light-induced scattering was improved considerably with the increase of the Li/Nb ratio. The relationship between the defect structures and the light-induced scattering was discussed.

1. Introduction

Lithium niobate ($LiNbO_3$, LN) crystals are among the most widely used functional materials in electro-optic, holographic storage and other nonlinear optics-related applications because of their excellent nonlinear optic properties. The large storage density and high diffraction efficiency of doped LN crystal make it very promising in holographic data storage application [1,2].

Among others, the most widely used is Fe:Mn:$LiNbO_3$ crystal [3]. However, a great challenge, light-induced scattering exists in congruent $LiNbO_3$ crystals limits their practical applications. To address this issue, an effective method is to suppress the light-induced scattering via doping optical-damage-resistance impurities such as AgO, MgO, and In_2O_3 in LN crystal [4–6]. In recent years, tetravalent ions (Hf^{4+}, Sn^{4+} and Zr^{4+}) were reported to be better choices in this regard than the ions mentioned above [7–9]. Some further experimental results identified that Zr^{4+} was a more favorable dopant in suppressing light-induced scattering in $LiNbO_3$ crystal, compared with Hf^{4+} or Sn^{4+} ions [10,11]. It is well accepted that intrinsic defects anti-site Nb defects (Nb ions occupying Li sites) and Li vacancies in $LiNbO_3$ crystals are the main causes to the light-induced scattering [12,13]. It is suggested that with the increase of Li/Nb ratios, the number of intrinsic defects will decrease remarkably and hence result in good optical properties [14–16].

In this work, ZrO_2 doped $LiNbO_3$:Fe:Mn crystals with varied Li/Nb ratios were grown by the Czochralski method. The measurement of ultraviolet–visible spectroscopy was used in probing the defect structures of the crystals. The Li/Nb ratio and the concentration of ZrO_2 in each crystal were determined with the inductively coupled plasma atomic emission spectrometry (ICP-AES). The light-induced scattering in these crystals was studied as a function of exposure energy. Finally, the mechanism of the relationship between the light-induced scattering and the Li/Nb ratios was discussed.

2. Experimental details

In order to produce crystals with high optical quality, Li_2CO_3, Nb_2O_5, ZrO_2, $MnCO_3$ and Fe_2O_3 with the purity over 99.99% were used as the origin oxides. The doping concentrations of ZrO_2, $MnCO_3$ and Fe_2O_3 were at 1.0 mol%, 0.10 wt% and 0.03 wt%, respectively. The Li/Nb ratios of the origin oxides in producing $LiNbO_3$:Fe:Mn:Zr were set as 0.94, 1.05, 1.20 and 1.38. All crystals were grown under the temperature gradient of 30 °C/cm above the melt, and detail optimized growth parameters were listed in Table 1. The as-grown crystals were transparent, and free of macro-defect or inclusion seen in them.

After growth, the crystals were slowly cooled down to room temperature at a rate of 50 °C/h. The crystals thus grown were then polarized in another furnace with a DC electric current density of 5.0 mA/cm^2 for 30 min. The middle parts of the poled crystals were cut into several 2.0 mm-thick specimens, with *y*-axis in their polishing surfaces, which are of optical grade for the characterization of optical properties.

We analyzed the concentration of Zr^{4+} and Li/Nb ratios in the crystals with an inductively coupled plasma atomic emission spectrometer (ICP-AES, Optima 5300DV). The ultraviolet–visible (UV–vis) absorption spectra of these samples were measured with the CARY UV–visible spectrophotometer with the spectral range from 300 to 900 nm.

In this work, exposure energy was employed as a measure in evaluating the resistance against the light-induced scattering in the doped $LiNbO_3$ crystals [17].

* Corresponding author. Tel.: +86 451 86413707; fax: +86 451 86488720.
E-mail addresses: yangchh@hit.edu.cn, xuchaochina@gmail.com (C. Yang).

0925-8388/$ – see front matter © 2011 Elsevier B.V. All rights reserved.
doi:10.1016/j.jallcom.2011.01.031

Table 1
Growth condition and composition of $LiNbO_3$:Fe:Mn:Zr crystals.

Sample	1#	2#	3#	4#
ZrO_2 in the melt (mol%)	1.0	1.0	1.0	1.0
ZrO_2 in the crystal (mol%)	0.964	0.915	1.004	0.989
Distribution coefficient (K_{eff}) of Zr	0.964	0.915	1.004	0.989
$MnCO_3$ in the melt (wt%)	0.10	0.10	0.10	0.10
Fe_2O_3 in the melt (wt%)	0.03	0.03	0.03	0.03
[Li]/[Nb] ratio in the melt	0.94	1.05	1.20	1.38
[Li]/[Nb] ratio in the crystal	0.930	0.954	0.979	0.991
Rotation rate (r/min)	18–22	18–22	20–25	27–30
Pulling rate (mm/h)	2.0	2.0	1.0	0.5

With this method, light-induced scattering dynamics were taken with irradiation time. One can see it was of a quantitative analysis in measuring light-induced scattering. The experimental setup was shown in Fig. 1. An extraordinary polarized beam of 532 nm in wavelength of 532 nm shone onto the samples to form a 2 mm diameter facula. A continuously tunable neutral density filter (NF) was utilized in varying incident intensity. The scattering light was blocked by a light shed and only the transmitted light was received by the photo-detector.

3. Results and discussion

3.1. Crystal composition

The results of ICP-AES are listed in Table 1. The effective distribution coefficient (K_{eff}) of Zr was obtained via comparing the measured Zr concentration in the $LiNbO_3$ crystal with the pre-set Zr concentration in the melt. It can be found that the effective distribution coefficient of Zr dopant is close to one, indicating that Zr distributes uniformly in crystal. In addition, the Li/Nb ratios in the crystals have the same tendency as those in the melts. Near-stoichiometric $LiNbO_3$ crystal can be obtained when the Li/Nb ratio approaches 1.38 in the melt.

3.2. UV–vis absorption spectra

Fig. 2(a) shows the UV–vis absorption spectra of the $LiNbO_3$:Fe:Mn:Zr crystals. Usually, the absorption edges of the crystals reflect the composition of the crystals and their defects, since their positions are sensitive to the Li/Nb ratios [18]. Fig. 2(b) illustrates the position of absorption edge versus Li/Nb ratios in the crystals. It can be seen from the figure that the absorption edges of $LiNbO_3$:Fe:Mn:Zr crystals shift to the violet first and then to red with the continuous increase of Li/Nb ratios. In our work, we use the band-edge position where the absorption coefficient is equal to 20 cm^{-1} as the criterion to compare the absorption edges of the samples [19,20].

In the Li-vacancy crystal structure model, the Li/Nb ratio of congruent lithium niobate is 0.94, consequently, the crystals are rich in Li vacancies. To maintain the electrical neutrality, some excessive Nb ions occupy vacant Li sites to form anti-site Nb_{Li}^{4+} defects in the crystals. In this paper, we use a parameter Z^{*2}/r to describe the phenomenon of the absorption edge shift, where $Z^* = Z - \sum s$, and Z^*, Z, $\sum s$ and r represent the effective nuclear charge number, the atomic

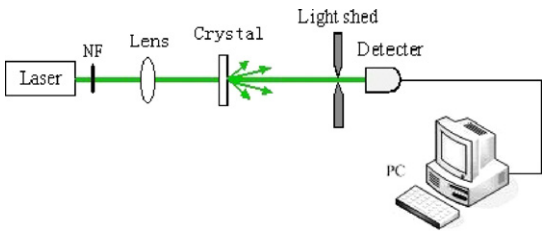

Fig. 1. Experimental setup for light-induced scattering measurement. NF: neutral filter.

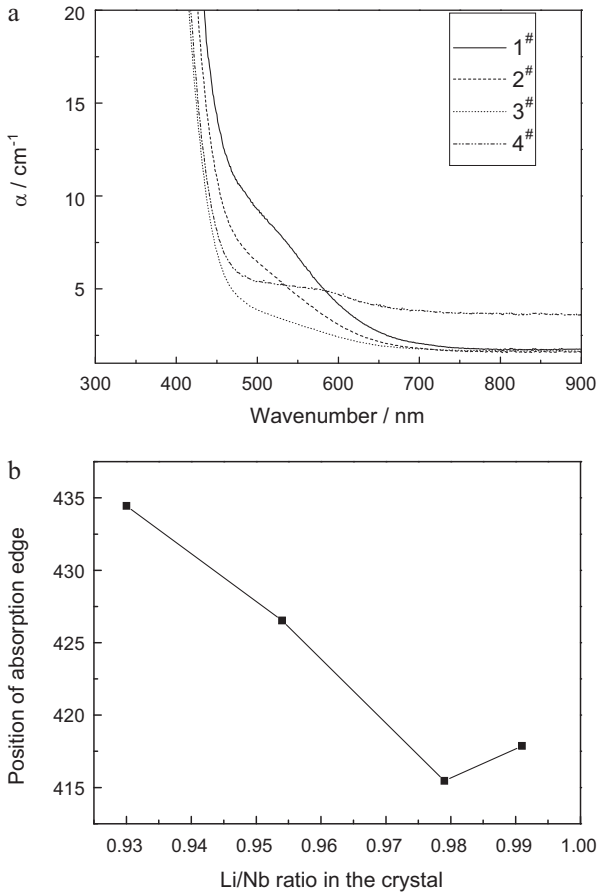

Fig. 2. (a) Measured ultraviolet–visible absorption spectra of $LiNbO_3$:Fe:Mn:Zr crystals and (b) optical absorption edge position versus Li/Nb ratio in crystal.

number of the ion, the shield factor and the radius of the ion, respectively. The fundamental absorption edge of the $LiNbO_3$ crystal is generated due to the valence electron transition from 2p orbital of O^{2-} to 4d orbital of Nb^{5+}. In that way, the valence electronic state of O^{2-} directly affects the position of the absorption edge. Hence the increasing ability of a neighboring doping ion to polarize an O^{2-} ion decreases the valence electron transition energy and results in the shift of the absorption edge to longer wavelength. The converse also applies [21]. The polarization ability values of Zr^{4+}, Mn^{2+}, Fe^{3+}, Li^+ and Nb^{5+} ions, given by $Z^* = Z - \sum s$, are 38.4, 34.45, 55.32, 2.49 and 58.51, respectively [22]. Apparently, the polarization ability of Nb^{5+} is higher than that of Zr^{4+}, Mn^{2+}, $Fe^{3+}$and Li^+. It is suggested that in Zr:Mn:Fe:$LiNbO_3$ crystals, Zr^{4+}, Mn^{2+} and Fe^{3+} ions substitute $Nb_{Li}{}^{4+}$ to form $Zr_{Li}{}^{3+}$, $Mn_{Li}{}^{+}$ and $Fe_{Li}{}^{2+}$, respectively. When increasing Li/Nb ratios in the melt, more Li^+ ions enter the crystal lattices and the concentration of $Nb_{Li}{}^{4+}$ decreases. This will reduce the deformation of surrounding O^{2-} ions, so the absorption edges shift to violet side. When the Li/Nb ratio in the crystal is larger than 0.979, $Nb_{Li}{}^{4+}$ almost disappears, and Zr^{4+} begin to enter normal Li sites. Since the Z^*-value of Zr^{4+} is higher than that of Li^+, the absorption edge of the crystal is redshifted.

3.3. Light-induced scattering

The dynamics of the transmitted light intensity in $LiNbO_3$:Fe:Mn:Zr crystals are shown in Fig. 3. The intensity of light-induced scattering is equal to $I_{T0} - I_{Tt}$, where I_{T0} and I_{Tt} are the transmitted light intensity at the instant when the incident light began to shine onto the sample, and that at time t, respectively. The strength of the light-induced scattering of

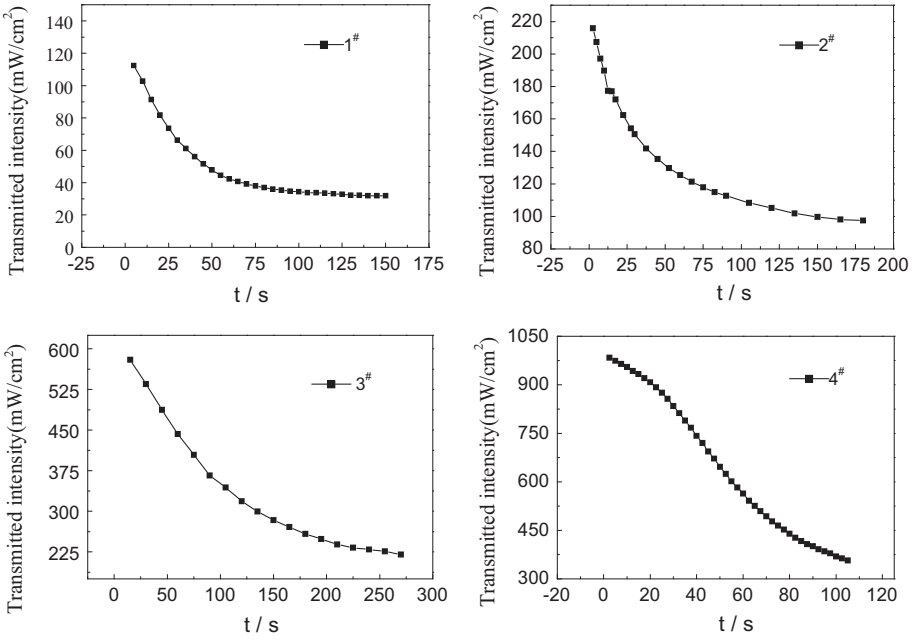

Fig. 3. Exposure time dependence of the light intensity transmitted from $LiNbO_3$:Fe:Mn:Zr crystals.

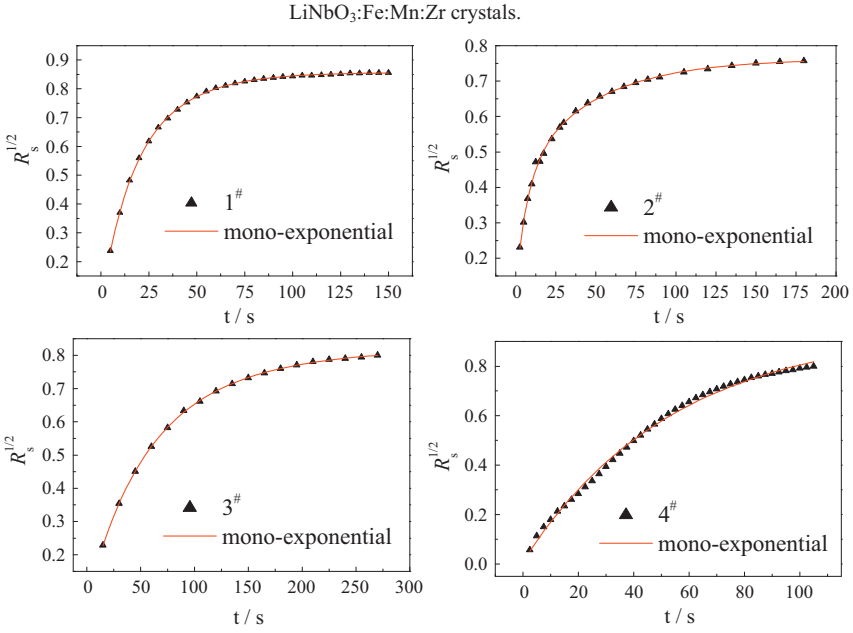

Fig. 4. Exposure time dependence of the scattering ratio of $LiNbO_3$:Fe:Mn:Zr crystals.

doped $LiNbO_3$ crystals is described by R_S, which is the ratio of scattering light intensity (I_S) to the incident light intensity (I_I). The experimental curves can be fitted by a mono-exponential function below

$$\sqrt{R_S} = \sqrt{R_{S,sat}}\left[1 - \exp\left(-\frac{t}{\tau}\right)\right] \quad (1)$$

where $R_{S,sat}$ is called the saturation scattering ratio, and τ is the scattering time constant. Here τ is defined as the time when the square root of scattering ratio $\sqrt{R_S}$ increases to $1 - 1/e$ of the square root of saturation scattering ratio $\sqrt{R_{S,sat}}$. The time constant τ can be obtained by fitting the dynamic curve according to Eq. (1) and the analyzed results are shown in Fig. 4.

Then the exposure energy (Er) can be calculated from

$$Er = I_{eff}\tau \quad (2)$$

where I_{eff} is the effective incident intensity.

Considered the reflectivity of the crystals, I_{eff} can be calculated by

$$I_{eff} = I - I_R = I(1 - R) \quad (3)$$

where R is the reflection index, and I is the total incident intensity. The value of R here is adapted from Ref. [17]. The results in regard with exposure energy are listed in Table 2. For comparison, we also list the values obtain in $LiNbO_3$:Fe:Mn and pure $LiNbO_3$ crystal under the same conditions. From Table 2 one can see that Sample 4# has the largest exposure energy of 23.81 J/cm^2. This value is approx-

Table 2
Parameters of illumination light intensity (I), exposure time (τ) and total exposure energy (Er) used for light-induced scattering measurements on $LiNbO_3$:Fe:Mn:Zr crystals.

Sample	I (mW/cm^2)	τ (s)	I_{eff} (mW/cm^2)	Er (J/cm^2)
1#	190.41	22.77	162.74	3.71
2#	357.33	34.86	305.41	10.65
3#	974.38	19.56	832.80	16.29
4#	1241.91	22.43	1061.46	23.81
$LiNbO_3$:Fe:Mn	76.43	15.60	65.32	1.02
Pure $LiNbO_3$	67.08	25.31	57.33	1.45

imately 7 times larger than that of Sample 1#, and 23 times larger than that of $LiNbO_3$:Fe:Mn crystal. By this simple comparison, it is seen that Sample 4# is a best choice in suppressing light-induced scattering.

The reason for enhancement of resistance to light-induced scattering can be explained as following. Here is the scalar expression

$$\partial \Delta n \approx \frac{Ak\alpha I}{\sigma} \quad (4)$$

where A is the generalized electro-optical coefficient, k the Glass constant, α the optical absorption coefficient, $\sigma = \sigma_{ph+}\sigma_d$ ($\sigma_{ph} \gg \sigma_d$, σ_d the dark conductivity, σ_{ph} the photoconductivity) and I the light intensity [23]. As the increase of the cation-vacancy photoconductivity, the photorefraction decreases due to the enhancement of the photoconductivity, whereas the photovoltaic current is nearly unchanged. If iron impurity is present, an abrupt decrease in the capture cross-section of Fe^{3+} acceptors should be responsible for the observed increase in σ_{ph}. $Nb_{Li}{}^{4+}$ is the most probable electron acceptor in the Li-deficient $LiNbO_3$ host. As the result, the reduced concentration of $Nb_{Li}{}^{4+}$ will leads to the increase of photoconductivity if the concentration of the concurrent Fe^{3+} acceptor is negligible [24]. In $LiNbO_3$ crystals, the enhancement of σ_{ph} can be attributed to the decrease of the concentration of $Nb_{Li}{}^{4+}$ as the site of Nb_{Li} is replaced by Zr^{4+} and Li^+. In $LiNbO_3$:Fe:Mn:Zr crystals with varied Li/Nb ratios, Zr^{4+} and Li^+ substitute $Nb_{Li}{}^{4+}$, and Fe^{3+} occupies Li site. When the concentration of ZrO_2 exceeds its threshold value, σ_{ph} rapidly increases because $Nb_{Li}{}^{4+}$ vanishes and most of the Fe ions substitute Nb^{5+}. The role of Mn ions in $LiNbO_3$:Fe:Mn:Zr crystals is the same as that of Fe ions. Consequently, the resistant capability against light-induced scattering in $LiNbO_3$:Fe:Mn:Zr crystals with the highest Li/Nb ratios (4#) is much better than that in other samples.

4. Conclusions

In summary, a series of $LiNbO_3$:Fe:Mn:Zr crystals with various Li/Nb ratios were grown. The results of UV–vis absorption spectra showed that the absorption edges of $LiNbO_3$:Fe:Mn:Zr crystals shifted to violet-side firstly and then to red-side when the Li/Nb ratios increased continuously, since more Li^+ cations enter the lattice and thus push $Zr_{Li}{}^{3+}$, $Mn_{Li}{}^{+}$ and $Fe_{Li}{}^{2+}$ to the normal Nb sites. From the experimental results of inductively coupled plasma atomic emission spectrometry it was found that the effective distribution coefficient of Zr was close to unity, and the Li/Nb ratio in the crystals had the same tendency as that in the melt. The results of incident exposure energy revealed that with the increase of Li/Nb ratio, higher incident exposure energy was needed to make the light in crystal scatter. Among the samples studied, sample 4# (Li/Nb = 0.991 in the crystal) was the best to resist the light-induced scattering and it can sustain energy density up to 23.81 J/cm^2, which is approximately 23 times higher than that of $LiNbO_3$:Fe:Mn crystal. This manifested the ability against light-induced scattering can be enhanced via tuning the Li/Nb ratio and doping concentration in the crystals. The photoconductivity was a key factor to understand the internal relationship between the defect structure and light-induced scattering of the crystals.

Acknowledgements

This work is financially supported by the National Natural Science Foundation of China under project No. 60777006 and the State Key Laboratory of Precision Measurement Technology and Instruments, Tsinghua University.

References

[1] X. Yue, A. Adibi, T. Hudson, K. Buse, J. Appl. Phys. 87 (2000) 4051.
[2] D.K. McMillen, T.D. Hudson, J. Wagner, Opt. Express 2 (1998) 491.
[3] K. Buse, A. Adibi, D. Psaltis, Nature 393 (1998) 665.
[4] M. Li, X. Liang, X. Xu, S.T.C.C. Solanki, J. Cryst. Growth 312 (2010) 3020.
[5] Y.X. Fan, H.T. Li, F.Y. Guo, Opt. Commun. 278 (2007) 413.
[6] Y. Kong, J. Wen, H. Wang, Appl. Phys. Lett. 66 (1995) 280.
[7] X.D. Sun, H.X. Shi, S.H. Luo, et al., Chin. Phys. B 19 (2010) 094209.
[8] L. Wang, S. Liu, Y. Kong, et al., Opt. Lett. 35 (2010) 883.
[9] Y.F. Kong, S.G. Liu, Y.J. Zhao, Appl. Phys. Lett. 91 (2007) 081908.
[10] N. Argiolas, M. Bazzan, M.V. Ciampolillo, et al., J. Appl. Phys. 108 (2010) 093508.
[11] F. Liu, Y. Kong, X. Ge, et al., Opt. Express 18 (2010) 6333.
[12] D. Xue, K. Kitamura, Solid State Commun. 122 (2002) 537.
[13] G. Malovichko, V. Grachev, O. Schirmer, Appl. Phys. B 68 (1999) 785.
[14] B. Lu, J. Xu, X. Li, et al., J. Alloys Compd. 449 (2008) 224.
[15] W.Y. Wang, X.L. Chen, D.Q. Ni, et al., J. Alloys Compd. 402 (2005) 224.
[16] S. Zhang, H. Xia, J. Wang, et al., J. Alloys Compd. 463 (2008) 446.
[17] X.D. Sun, S.H. Luo, J. Wang, et al., Opt. Mater. 31 (2009) 1678.
[18] S Yao, J. Wang, H. Liu, et al., J. Alloys Compd. 455 (2008) 501.
[19] I. Földvári, K. Polgár, R. Voszka, et al., Cryst. Res. Technol. 19 (1984) 1659.
[20] K. Polgár, Á. Péter, L. Kovacs, et al., J. Cryst. Growth 177 (1997) 211.
[21] Z.P. Xu, Y.H. Xu, Mater. Lett. 61 (2007) 3243.
[22] H.C. Lin, B. Yu, C. Xu, Proc. SPIE 7517 (2009) 75170K–75172K.
[23] T Volk, N. Rubinina, M. Wöhlecke, J. Opt. Soc. Am. B11 (1994) 1681.
[24] H. Donnerberg, S.M. Tomlinson, O.F. Schirmer, Phys. Rev. B 40 (1989) 11909.